Gene Expression, Vol. 14, pp. 83–100
Printed in the USA.

1052-2166/07 $90.00 + .00
E-ISSN 1555-3884
www.cognizantcommunication.com

Disruption of ZAS3 in Mice Alters NF-κB and AP-1 DNA Binding and T-Cell Development

CARL E. ALLEN,*† JOHN RICHARDS,‡ NATARAJAN MUTHUSAMY,§ HERBERT AUER,*
YANG LIU,‡ MICHAEL L. ROBINSON,* JOHN A. BARNARD,* AND LAI-CHU WU†§¶

**Department of Pediatrics and Center for Cell and Developmental Biology, Columbus Children's Research Institute, Columbus, OH 43205, USA*
†Molecular, Cellular and Developmental Biology Program, The Ohio State University, Columbus, OH 43210, USA
‡Department of Pathology, The Ohio State University, Columbus, OH 43210, USA
§Department of Internal Medicine, The Ohio State University, Columbus, OH 43210, USA
¶Department of Molecular and Cellular Biochemistry, The Ohio State University, Columbus, OH 43210, USA

The large zinc finger proteins, ZAS, regulate the transcription of a variety of genes involved in cell growth, development, and metastasis. They also function in the signal transduction of the TGF-β and TNF-α pathways. However, the endogenous protein of a representative member, ZAS3, is rapidly degraded in primary lymphocytes, which limits the determination of its physiological function in vitro. Therefore, we have generated mice with targeted disruption of *ZAS3*. Oligonucleotide-based microarray analyses revealed subtle but consistent differences in the expression of genes, many of which are associated with receptor or signal transduction activities between *ZAS3*$^{+/+}$ and *ZAS3*$^{-/-}$ thymi. Gel mobility shift assays showed altered DNA binding activities of NF-κB and AP-1 proteins in ZAS3-deficient tissues, including the thymus. Lymphocyte analysis suggested a subtle but broad function of ZAS3 in regulating T-cell development and activation. In CD3+ *ZAS3*$^{-/-}$ thymocytes, the CD4/CD8 ratio was decreased and CD69 expression was decreased. In peripheral CD4+ *ZAS3*$^{-/-}$ lymphocytes we observed an increased number of memory T cells.

Key words: Transcription; Signal transduction; Gene regulation; Zinc finger proteins; T-cell development

INTRODUCTION

The HIVEP/ZAS/Shn family of transcriptional and signaling molecules includes three paralogous proteins in mammals: ZAS1 (also known as HIV-EP1, MBP-1, PRDII-BF1, αA-CRYBP1, and Shn-1), ZAS2 (also known as HIV-EP2, MBP-2, MIBP1, and Shn-2), and ZAS3 (also known as HIV-EP3, KRC, KBP-1, and Shn-3) [reviewed in (4,45)]. However, there is only a single ZAS homolog in invertebrates, including Schurri (shn) in *Drosophila melanogaster* and SMA-9 in *C. elegans*. The ZAS proteins are unusually large transcriptional proteins of more than 2500 amino acid residues. Each ZAS protein typically contains two widely separated zinc finger pairs that individually bind to specific DNA sequences, including the κB motif (1). The κB motif, interacting with NF-κB as well as ZAS proteins, is a *cis*-acting enhancer element that regulates transcription of genes involved in immunity, differentiation, growth, and proliferation (7). While NF-κB typically activates transcription, ZAS proteins can activate or repress transcription depending on the gene context (4).

Biochemical and genetic studies identified ZAS proteins as transcription regulators and signaling molecules with pleiotropic functions. In *Dropsophila*, shn controls fundamental developmental processes such as dorso-ventral patterning during embryonic devel-

Address correspondence to Lai-Chu Wu, Department of Internal Medicine, The Ohio State University, 480 Medical Center Drive, Columbus, OH 43210, USA. Tel: 614-293-3042; Fax: 614-293-5631; E-mail: laichu.wu@osumc.edu

opment, proliferation and differentiation of the wing, and maintenance of germline stem cells (38,43,44). In *C. elegans*, SMA-9 regulates body size, male tail pattern, and mesodermal patterning (13,37). The functions of shn and SMA-9 are mediated through BMP/TGF-β-related signaling cascades. Recently, two mammalian counterparts, ZAS1/Shn1 and ZAS2/Shn-2, have been shown to mediate BMP signaling by binding to Smad1 and Smad4 (22,48). Furthermore, the Shn-2 and Smad1/4 complex interacts with C/EBP-α to induce the expression of PPARγ2, which has a critical role in adipogenesis (22). Involvement of ZAS3 in the TGF-β pathway has not yet been reported; however, ZAS3 has been shown to interact with TRAF2 to regulate TNF-α-driven responses (33), to inhibit NF-κB nuclear translocation (17), and to interact with c-Jun to regulate AP-1 activity (34).

Besides the κB motif, each ZAS protein also binds specifically to other unrelated DNA sequences (1,45). ZAS3 was initially cloned due to the ability of its gene products to bind the recombination signal sequences (RSS) (47). RSS contains conserved DNA elements that mediate the somatic recombination of the immunoglobulin and T-cell receptor (TCR) gene segments to generate immune diversity (14). Subsequent in vitro experiments showed that ZAS3 was the major RSS-binding protein in B lymphocytic cell lines and that its affinity for the RSS decreased upon V(D)J recombination (46). The lymphoid-specific expression and RSS-binding properties prompted us to speculate that ZAS3 may be involved in lymphoid development and/or function. However, in preliminary experiments using primary lymphocyte cultures from both thymus and spleen, we observed a dramatic decrease in ZAS3 transcripts and proteins within hours of ex vivo cultivation. Therefore, in order to study the function of ZAS3 in lymphocytes in vivo, we developed an animal model, a *ZAS3*$^{-/-}$ mouse, by homologous recombination.

ZAS3$^{-/-}$ mice were viable and with life spans comparable to control mice. Consistent with our previous finding in *ZAS3*$^{-/-}$*;RAG2*$^{-/-}$ chimeric mice (2), ZAS3 deficiency did not impact T-cell proliferation or TCR-β chain somatic recombination. Relative to control mice, *ZAS3*$^{-/-}$ mice exhibited differences in the expression of specific genes, altered NF-κB and AP-1 binding activities, and skewed T-cell populations. Compared to wild-type mice, CD3+ thymocytes of *ZAS3*$^{-/-}$ mice exhibited decreased CD4/CD8 ratio and reduced CD69 expression. Additionally, CD44^{hi}/CD62L^{lo} subset and CD25 and CD69 expression were increased in CD4+ splenocytes of *ZAS3*$^{-/-}$ mice. In agreement with a recent report (23), we also observed a progressive increase in bone density of *ZAS3*$^{-/-}$ mice. The subtle defects observed in ZAS2- and ZAS3-deficient mice compared with the dramatic developmental defects and subsequent embryonic lethality that results from disruption of *shn* in *Drosophila* suggest the mammalian ZAS proteins may have redundant functions, which may be uncovered with deletion of two or more ZAS genes in a single animal.

MATERIALS AND METHODS

Antibodies

ZAS3 antisera have been described previously (6). Other antibodies purchased were: CD4, CD8, CD62L, CD44, CD3, CD25, and CD69 (eBioscience, San Diego, CA); anti-BrdU (BD Biosciences, San Jose, CA); and actin, p65, histone H1, and p-IκB antibodies (Santa Cruz Biotechnology, Santa Cruz, CA).

Generation of ZAS3$^{-/-}$ *Mice*

All mice were maintained in a sterile Biosafety Level 2 animal facility with protocols approved by the Institutional Animal Care and Use Committee at the Columbus Children's Research Institute. The targeting vector was designed to replace a 484-bp region of the ZAS3 gene encoding the first zinc finger pairs with a neomycin cassette. Both the targeting vector and heterozygous ZAS3 embryonic stem (ES) cells have been described previously (2). Blastocysts of C57BL/6 mice were injected with heterozygous (*ZAS3*$^{+/-}$) ES cells and then implanted into the uteri of 4–6-week-old pseudopregnant surrogates according to standard protocols (16). Chimeric males, evident by mixed coat color derived from both the C57BL/6 blastocyst (black) and injected 129Sv/J-derived ES cells (agouti), were bred with C57BL/6 females for germline transmission to obtain heterozygous *ZAS3* offspring. Subsequently, homozygous *ZAS3*$^{-/-}$ mice were established by breeding heterozygous *ZAS3* mice. Phenotypic variability in *ZAS3*$^{-/-}$ mice in a mixed C57BL/6J × 129/Sv genetic background prompted the establishment of a *ZAS3*$^{-/-}$ congenic mouse line on a C57BL/6 genetic background to minimize the influence of segregating genetic modifier alleles. Heterozygous *ZAS3* female offspring were backcrossed with wild-type C57BL/6 males for eight generations (N8). Mice from the eighth generation were intercrossed and experiments described in this report were performed with mice derived from that colony.

Southern Blot Analyses

Genomic DNA isolated from mouse tail pieces was digested with *Kpn*I or *Eco*RI, resolved by 0.8% agar-

ose gel electrophoresis, and transferred onto a nylon membrane. Hybridizations were performed using [^{32}P]dCTP-labeled ZAS3 cDNA fragments, and signals were visualized by autoradiography.

Histological Analyses

Tissues or organs were fixed overnight in 4% paraformaldehyde/PBS at 4°C, dehydrated through a graded series of ethanol baths, and embedded in paraffin wax. The paraffin blocks were cut into 8-μM-thick sections and adhered to glass slides. The slides were dewaxed, stained with hematoxylin and eosin, mounted with Permount, examined and photographed under a Zeiss microscope (Zeiss, Jena, Germany) in the Mouse Phenotyping Core Facility of The Ohio State University Comprehensive Cancer Center (OSUCCC).

Isolation and Cultivation of Lymphocytes

Thymocytes and splenocytes were isolated from four 3-month-old C57BL/6 male mice. A fraction (~10%) of individual tissues was first dissected out and immediately immersed in liquid nitrogen for RNA and protein preparation. The remaining tissues were pooled in 5 ml of ice-cold DMEM with 10% FBS (Invitrogen, Carlsbad, CA), and pushed through a 70-μm pore size cell strainer. Filtered cells were further purified using Ficoll-Paque™ (Amersham Biosciences, Piscataway, NJ) gradient, and washed with 10 ml of ice-cold PBS twice. Duplicate cell samples (1×10^6 cells) were incubated in 35-mm tissue culture plates with 6 ml of DMEM supplemented with 10% FBS, 2 mM glutamine, and 50 μM β-mercaptoethanol at 37°C and 5% CO_2. RNA and protein samples were isolated from cultured cells (1 ml) harvested at each time interval of 0, 2, 6, 12, and 24 h.

RNA and Protein Extraction

Total RNA was isolated from cells and tissues with Trizol (Invitrogen) and then purified with an RNEasy Kit™ (Qiagen Inc, Valencia, CA). Total protein lysates and nuclear extracts were isolated from cells with M-PER reagent and NE-PER reagent, respectively (Pierce, Rockford, IL), supplemented with protease inhibitors cocktail (Roche, Indianapolis, IN), and stored at −80°C.

Analysis of T-Cell Receptor Diversity With Array Technology

Total RNA was isolated from whole thymus and its integrity was verified with an Agilent Bioanalyzer. The level of diversity of TCR-β chain was measured using T7 promoter linked to a mouse TCR Cβ reverse primer (T7 + Cβ) for first-strand synthesis using an array-based strategy (32), performed in the OSUCCC Microarray Shared Resource. Second-strand synthesis and preparation of biotin-labeled cRNA were conducted according to standard protocols (Affymetrix Inc., Santa Clara, CA). Equal amounts of cRNA from duplicated wild-type and *ZAS3*$^{-/-}$ samples were hybridized to human genome U133A 2.0 gene chips (Affymetrix Inc.). The human oligonucleotide sequences served as random sequence targets for the mouse TCR variable region cRNA probes. For each gene chip experiment, raw data corresponding to oligonucleotide location and hybridization intensity were first obtained, and the number of oligonucleotide locations with intensity above background (presented as percent of *P call* in Table 2) was summed.

Western Blot Analysis

Proteins (30 μg) were resolved by 4–20% SDS-PAGE, transferred onto Hybond nitrocellulose membrane (Amersham Biosciences) or PVDF membranes (Pierce Biotechnology, Inc. Rockford, IL), incubated with appropriate primary antibodies, washed, and then incubated with secondary antibodies conjugated with horseradish peroxidase. Signals developed with SuperSignal West Dura Extended Duration Substrate (Pierce Biotechnology) were obtained by exposing protein filters to X-ray films. The quality and amount of protein samples were examined routinely by reversibly staining the protein gels (E-Zinc Reversible Stain Kit; Pierce) before transferring onto membranes.

Electrophoretic Mobility Shift Assays (EMSA)

EMSA using α-^{32}P-labeled κB (5′-CCGGGG GGACTTTCCGCTCCAC-3′) or AP-1 (5′-CCGGAT TGAGTCACGCTTCCAC-3′) double stranded oligonucleotides supplemented with excess nonspecific DNA competitor poly(dI-dC) (Sigma-Aldrich) were performed as described previously (17).

Microarray Analysis of Gene Expression

Five independent microarray hybridizations were performed with thymi isolated from sex- and age-matched mutant and wild-type littermates at 6–8 weeks of age. The Agilent Whole Mouse Genome Oligo Microarray (G4121A) containing over 20,000 60-mer oligonucleotide probes representing mouse genes, ESTs, and EST clusters was used (Agilent, Cincinnati, OH). Probe labeling and hybridization were preformed by the Microarray Core Facility (Columbus Children's Research Institute) following the manufacturer's protocols. Briefly, cDNA probes were synthesized with Superscript III, oligo-dT primers,

and dNTPs supplemented with amino-allyl-UTP to improve hybridization characteristics and stability. After purification, cDNA samples from mutant or control mice were labeled with Cy5 or Cy3, respectively, and hybridized to the microarray for 14 h at 48°C. Slide image was acquired using an Affymetrix 428 scanner with gain settings set so that 95% of spots were below saturation to yield the maximum dynamic range within an experiment. Images were converted into ".gpr" files using GenePix software (Molecular Devices, Sunnyvale, CA). Complete data sets including ".gpr" files were deposited onto the Gene Expression Omnibus website (http://www.ncbi.nlm.nih.gov/geo) with the Series Accession Number GSE6570.

Normalization and Analysis of Microarray Data

Data were analyzed using GeneTraffic 2.6 software (Iobion, La Jolla, CA). Lowess-global normalization was applied to all experiments. Flagging parameters were set as spot intensity lower than the intensity of local spot background, spot intensity lower than average background, and raw spot intensity less than 100. Flagged spots were not included in normalization or aggregate calculations. Only genes that were induced or repressed over 1.5-fold in at least four of the five independent analyses and hybridization were targeted for potential further study. The NIA Array Analysis Tool (http://lgsun.grc.nia.nih.gov) was used to determine the false discovery rate (FDR), which is equivalent to a *p*-value in experiments with multiple hypothesis testing. The maximum FDR was set at 0.05. The NIA Array Analysis Tool was also used to determine the correlation coefficient matrix for each of the experiment sets. Analysis of overrepresentation of genes differentially expressed in ZAS3-null mice was performed with the Expression Analysis Systematic Explorer (EASE) program (18). Input included all genes upregulated or downregulated over 1.5-fold in the array experiments described above. Parameters were EASE score <0.05 and False Discovery Rate equal to 0.

Quantitative Real-Time PCR

Real-time PCR was performed using an ABI 7000 DNA sequence detection system (Applied Biosystems, Foster City, CA). Total RNA (1 μg) was reverse transcribed using oligo-dT primers and SuperScript III RT (Invitrogen). Complementary DNA was amplified using primer sets and Sybr Green Master Mix (Applied Biosystems) in 96-well plates. Appropriate primer sequences were designed from published murine sequences in GeneBank using PrimerDesigner software (ABI). The experiments were performed thrice and similar results were obtained. Results were reported as ΔCt relative to a control, GAPDH. For each experiment the ΔCt was determined by the average of triplicate cDNA samples. Primer sequences are show in TABLE 1.

Cell Proliferation and Flow Cytometry

Proliferation of splenocytes and thymocytes in mice (3–5 months old) were assessed by BrdU incorporation as described previously (35). For flow cytometry analysis of cluster of differentiation (CD) markers, red blood cell-depleted single cell suspensions were prepared from thymus and spleen isolated from three pairs of age (3 months old)- and sex-matched siblings. Cells were initially incubated with monoclonal antibodies 2.4G2 supernatant to block nonspecific antibody binding, and then stained with appropriate fluorochrome-conjugated monoclonal antibodies (Pharmingen, San Diego, CA), fixed, and analyzed with a FACSCalibur (Becton Dickenson, San Jose, CA). Differences in the values between the mutant and wild-type controls were analyzed statistically using Student's *t*-test.

RESULTS AND DISCUSSION

ZAS3 Expression in Primary Lymphocytes Is Abrogated During In Vitro Cultivation

Microarray analysis has shown that the expression of many genes changes upon in vitro culturing of human peripheral blood mononuclear cells (12). Therefore, prior to proceeding with in vitro studies to determine the function of ZAS3 using primary lymphocytes, we evaluated ZAS3 expression in normal lymphocytes upon tissue culture cultivation. Thymocytes, purified and pooled from four 3-month-old wild-type C57BL/6 mice and maintained under standard tissue culture conditions, were harvested at various times over a 24-h period. Real-time PCR analysis showed that the expression of ZAS3 transcripts decreased dramatically in culture to less than 50-fold after 6 h and continued to decrease to over 300-fold by 24 h (Fig. 1A). Western blot analysis also showed that the levels of ZAS3 protein in thymocytes decreased significantly after 12 h of cultivation and was beyond detection by 24 h (Fig. 1B). A similar reduction in ZAS3 protein expression over time was observed in cultured splenocytes (Fig. 1C). As a control, the protein filters were incubated with actin antibodies. The decreased in actin at 24 h probably represented decreased number of cells with time due

TABLE 1
PRIMER SEQUENCES

Gene	Forward Primer	Reverse Primer	Amplicon Size (bp)	Accession No.
ZAS3	TTTTGGTCATCGGAAGTGGTG	TGGAGAATAGCAGCCTCAGAGG	69	AY454345
ZAS3	TCGAAGGAGGGTACAAATCAAAC	CCGCGGCCTCGCACATAT	51	AY454345
Ephrin A1	TCCCCAAGGAAGCCATAATG	TCCCCCGCAGGAAGCT	69	NM_010107
NK2	CCGCCGGGATTTATTGAGT	TGACCGGGCTTGGTAACATC	68	NM_008699.2
Glomulin	TGTTCAGGGCATCGGTATTG	TCCATGTTCAACTGCAGAAGGT	73	BC003446.1
JAK1	ACTGCAGATGCCCACCATTAC	TGGCAGCCGTTCTGTATATTGT	66	NM_146145.1
Trim30	GCTGGCTTTGTGAGCGATCT	TTCTTGGTCAACCTCTTCAATGAG	70	AF220015
RAG1	TTGTCTTCCACTCCATAACCAGAA	TGGACCGCCAGACCTCATA	65	AY011883.1
GAPDH	CATGGCCTTCCGTGTTCCTA	GCGGCACGTCAGATCCA	54	BC083065

to cell death in culture. Compared to actin, the reduction of ZAS3 was more pronounced and ZAS3 proteins were undetectable at 24 h (Fig. 1B, C, lower panels).

The pronounced decrease in ZAS3 expression in primary lymphocytes ex vivo may explain the failure of a previous report to detect ZAS3/KRC transcripts in unstimulated CD4+ T cells by RT-PCR (34), though ZAS3/KRC is expressed robustly in thymus and lymphocytes in vivo (15). It is likely that ZAS3 expression was lost during cell isolation and cultivation. Nevertheless, the expression of ZAS3 in CD4+ T cells has been reported to be maintained and induced in tissue culture by the cytokine IL-2 (34), or by the non-tumor-promoting phorbol ester, prostratin (39). The loss of ZAS3 expression under standard tissue culture conditions also suggests the sensitivity of the gene regulation of ZAS3 to environmental factors. Isolated cells grown in suspensions lack the three-dimensional architecture, cell–cell interactions, and the extracellular matrix of intact tissues or whole organs. Because ZAS3 suppresses cell proliferation (3), downregulation of ZAS3 might favor adaptation of primary lymphocytes to a new in vitro environment. Because of the heterogeneity of primary lymphocyte populations, the substantial decline in ZAS3 expression could also reflect the short life span of ZAS3-expressing lymphocytes ex vivo, specific transcriptional repression of ZAS3 induced by tissue culture conditions, or both. The rapid and pronounced decline of ZAS3 expression upon ex vivo cultivation demonstrates the limitations of using primary cell culture systems to evaluate the physiological function of ZAS3.

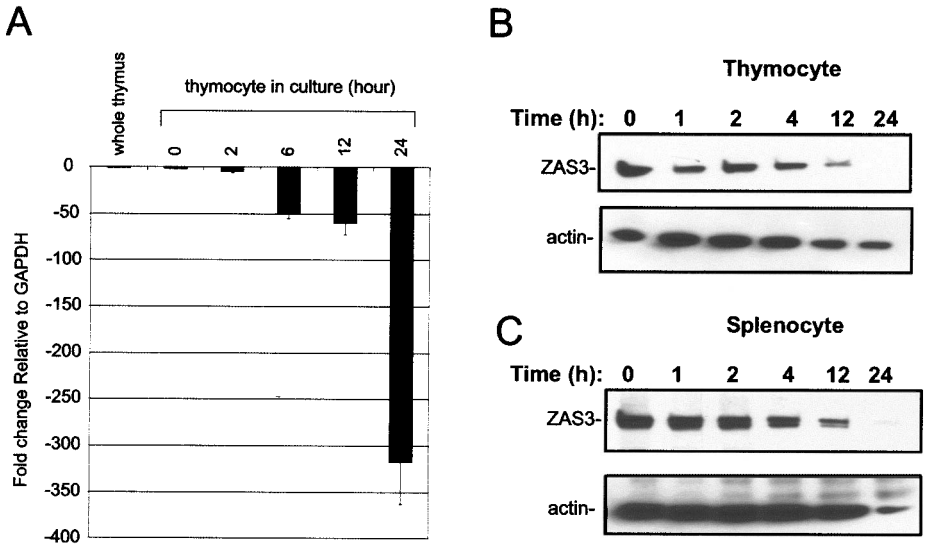

Figure 1. Loss of ZAS3 mRNA and protein expression upon tissue culture cultivation. (A) Real-time PCR analysis for ZAS3 mRNA from freshly isolated whole thymus and primary thymocytes cultured at time intervals indicated on the top of each lane. The results shown are derived from two independent experiments and normalized to GAPDH expression using the ΔCt method. (B, C) Western blot analysis of nuclear extracts of thymocytes (B) and splenocytes (C). Protein filters were also hybridized with actin antibodies as a control.

Generation of ZAS3$^{-/-}$ *Mice*

The ZAS3 protein harbors five zinc fingers, which are organized into two widely separated pairs and a middle solitary zinc finger (Fig. 2A). The targeting vector, pS7-neo, was designed to disrupt ZAS3 production by replacing a DNA region encoding the first zinc finger pair with a neomycin cassette (Fig. 2A). The vector was introduced into 129Sv/J ES cells and, subsequently, two independent heterozygous *ZAS3* ES cell lines were established (2). Heterozygous *ZAS3* ES cells were injected into blastocysts of C57BL/6 mice to generate chimeric mice. Male chimeric mice were crossed with C57BL/6 female mice. Heterozygous *ZAS3* mice obtained after successful germline transmission were then intercrossed to obtain homozygous mice. Targeted disruption of the ZAS3 mutant allele was validated by Southern blot analysis of genomic DNA prepared from mouse tails and hybridization probes flanking both sides of the targeted region (Fig. 2B). In Southern blots using a hybridization probe (probe a) located upstream of the targeted region, the wild-type *ZAS3* allele yielded signals of a 5.5-kb *Kpn*I fragment, whereas the mutated allele yielded a larger fragment of 6.5 kb. Similarly, *Eco*RI digests and a probe located downstream (probe b) of the deleted region yielded signals of 3.1 and 4.1 kb for wild-type allele and mutant allele, respectively. The loss of ZAS3 protein production in *ZAS3*$^{-/-}$ mice was demonstrated by Western blot anal-

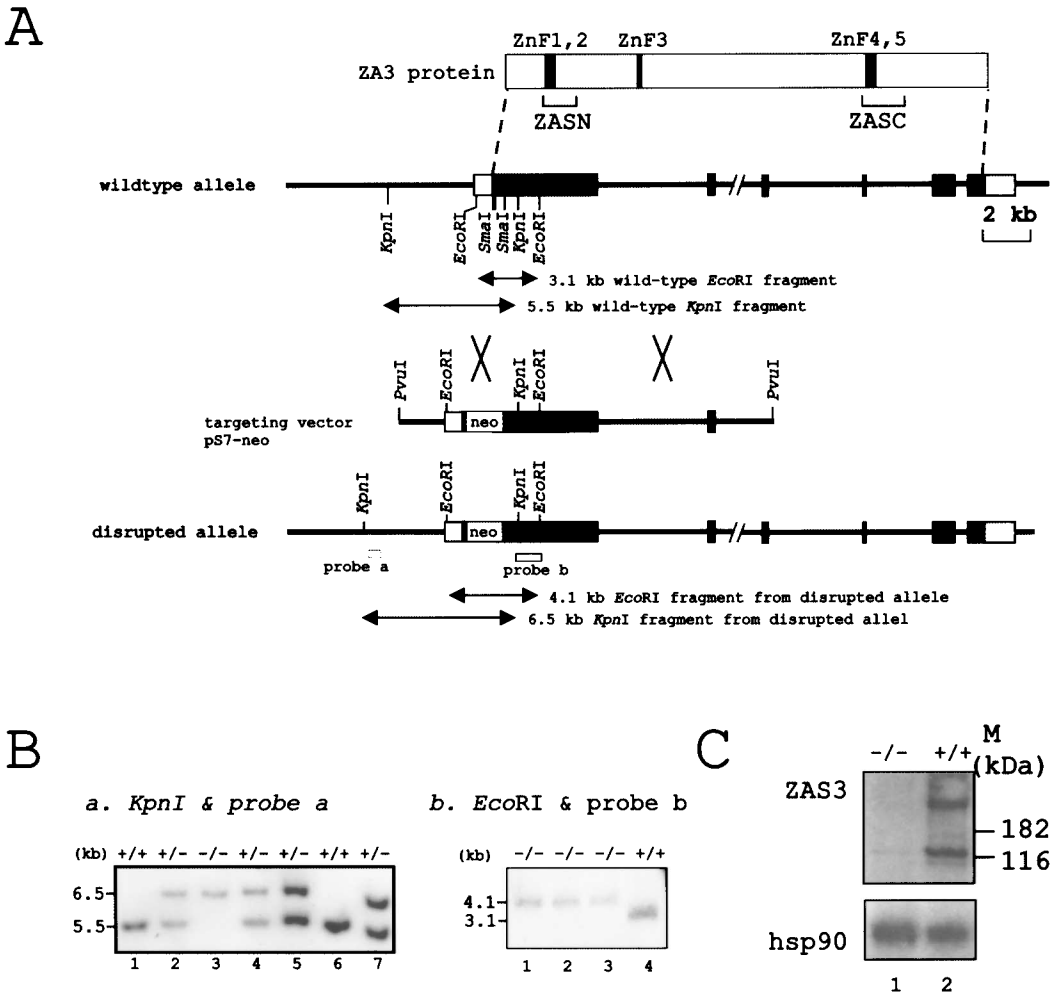

Figure 2. Generation and characterization of ZAS3 knockout mice. (A) Schematic presentation of the gene targeting of ZAS3 by homologous recombination. The targeting vector, pS7-neo, is designed to disrupt ZAS3 production by replacing a portion of the ZAS3 protein-coding region with a neo-cassette. Black boxes: protein-coding regions; white boxes: untranslated regions; neo: neo-cassette. (B) Diagnostic Southern blot analyses. Genomic DNA prepared from mouse tails were digested with (a) *Kpn*I and hybridized with probe a. The wild-type *ZAS3* allele yielded signals of 5.5 kb, whereas the mutated allele yielded signals of 6.5 kb; and (b) *Eco*RI and probe b. The wild-type *ZAS3* allele yielded signals of 3.1 kb and the mutant allele 4.1 kb. (C) Western blot analysis. Thymic protein lysates resolved by SDS-PAGE were subjected to Western blot analysis using ZAS3 antiserum (upper panel). The filter was also incubated with hsp90 antibodies as a loading control (lower panel).

ysis using ZAS3 antisera. Protein species of 260 and 115 kDa were observed from thymus of wild-type mice but not from *ZAS3*$^{-/-}$ mice. Expression of control protein, hsp90, was similar in both samples (Fig. 2C).

Throughout the process of establishing the *ZAS3*$^{-/-}$ mouse line, we observed a variety of phenotypes in *ZAS3* heterozygous and homozygous mice in mixed 129Sv/J and C57BL/6 background including polydactyly, smaller body size, variable spleen size, kyphosis, and extensive apoptosis of thymocytes (data not shown). However, while those phenotypes were reproducible, they were sporadic. The inconsistent phenotypes could be due to genetic modifier effects caused by mixed genetic backgrounds in the *ZAS3*$^{-/-}$ mice. In many mouse knockout models, the phenotype of gene mutations can be modulated by the genetic background (30). For example, knockout mice of another ZAS gene, *ZAS2/shn2*, derived from TT2 ES cells (C57BL/6 × CBA) and C57BL/6 mice had severe depletion of CD4+ and CD8+ cells due to the impairment of positive thymic selection (41). However, when the *ZAS2* mutated alleles were placed in the BALB/c background, those mice had moderate numbers of CD4 and CD8 T cells (25). Therefore, in order to minimize influence of genetic variability due to mouse strain, the *ZAS3* mutated allele was backcrossed for eight generations (N8) to a C57BL/6 background. Heterozygous *ZAS3* breeding pairs were then established, and all further studies reported here used mice derived from that colony.

ZAS3 Deficiency Did Not Affect Histological Features of Immune Tissues or Adipogenesis

As with *ZAS2*$^{-/-}$ mice (25), there are no gross anomalies in the major organs of *ZAS3*$^{-/-}$ mice. The histology of primary immune organs of *ZAS3*$^{-/-}$ mice including thymus, spleen, lymph nodes, and Peyer's patch were similar to wild-type (Fig. 3). We also examined the adipose tissues of *ZAS3*$^{-/-}$ mice because ZAS2/Shn2-knockout mice had reduced white adipose tissues and body weight (22). Decreased adipose was attributed to cooperation of ZAS/Shn2 with the Smad proteins of the TGF-β pathway and with C/EBP-α to positively regulate the expression of PPARγ2, a key transcription factor for adipocyte differentiation (22). That study also showed that the epididymal fat of *Shn-2*$^{-/-}$ mice was markedly reduced, with some adipocytes showing a preadipocyte-like phenotype (22). However, the overall body weight and fat content of *ZAS3*$^{-/-}$ mice were comparable to wild-type siblings. The histology of the epididymal fat pad was also similar between *ZAS3*$^{-/-}$ mice and control mice, with a typical large lipid droplet occupying most of the cytoplasm and the nucleus compressed and displaced to one edge (Fig. 3). Thus, ZAS3 deficiency does not affect adipogenesis, suggesting a functional divergence of ZAS2 and ZAS3.

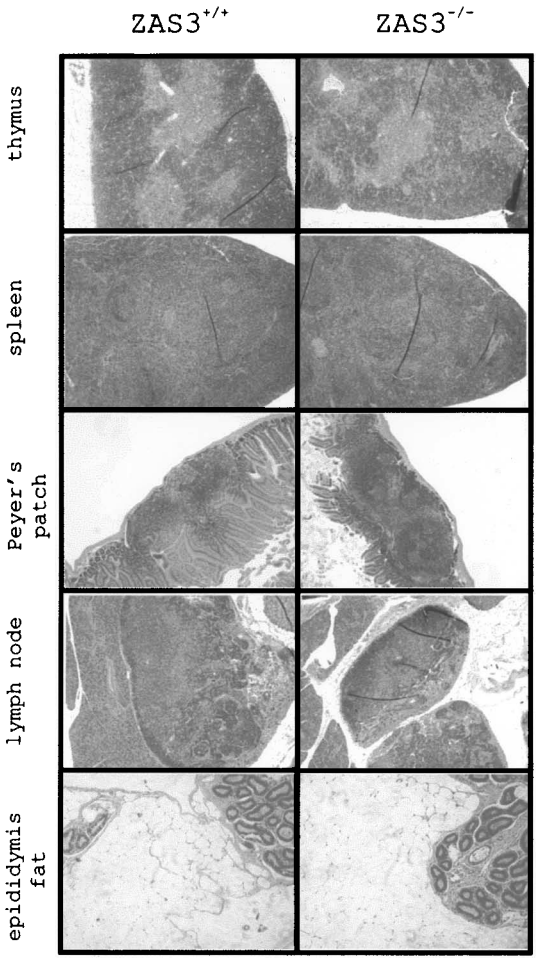

Figure 3. Histological analysis of thymus, spleen, Peyer's patch, lymph node, and adipose tissues. Tissue sections of control *ZAS3*$^{+/+}$ (left panels) and *ZAS3*$^{-/-}$ (right panels) mice were stained with hematoxylin and eosin. No notable differences in the histology between control and *ZAS3*$^{-/-}$ tissues were observed.

ZAS3 Deficiency Did Not Affect Lymphocyte Proliferation or T-Cell Receptor Diversity

We examined lymphocyte proliferation and development of *ZAS3*$^{-/-}$ mice. Several lines of evidence suggest that ZAS3 has a tumor suppressor function. First, downregulation of ZAS3 in tissue cultured cells led to cell proliferation and anchorage-independent growth, a phenotype of transformed cells (3). Second, a malignant tumor formed spontaneously in a *ZAS3*$^{-/-}$/*RAG2*$^{-/-}$ chimeric mouse (2). Third, downregulation and loss of heterozygosity of ZAS3 were found in lymphomas generated by retroviral insertional muta-

genesis in AKXD-Blm$^{m3/m3}$ mice (40). However, in the C57BL/6 backcrossed ZAS3-null mice, no significant difference in the life span and body size or weight was observed when compared to wild-type littermates.

To evaluate whether ZAS3 deficiency modulated proliferation of lymphocytes in vivo, we compared splenocyte proliferation between ZAS3-deficient and wild-type control mice. Mice (3–5 months old) were pulsed with the nucleotide analogue BrdU. Three hours later, splenocytes were isolated and analyzed for BrdU incorporation in CD4+ or CD8+ cells by flow cytometry. There were no significant differences in BrdU incorporation, which reflected similar proliferation rate between splenocytes of the two mouse groups (Fig. 4A, B). Thus, the lack of ZAS3 did not affect the basal proliferation of unstimulated splenic T cells in our knockout mouse model.

ZAS3 was initially cloned due to the ability of its gene products to bind the conserved recombination signal sequences (RSS) that mediate somatic V(D)J recombination of immunoglobulin and TCR variable region gene segments (19). The RSS-binding specificity of ZAS3 was subsequently confirmed by methylation interference analysis (19) and by site selection assays (1). Southwestern blot analysis of pre-B cells nuclear extracts showed that a 115-kDa protein species that reacted with ZAS3 antisera was the major RSS-binding species and that its RSS-binding affinity decreased upon V(D)J recombination (46). That 115-kDa species is probably a ZAS3 protein isoform, which was also observed in the thymus of wild-type but not in *ZAS3*$^{-/-}$ mice (Fig. 1C). Furthermore, in situ hybridization experiments of developing mouse embryos showed that synthesis of ZAS3 transcripts began at embryonic day E14.5 at the cortical region of the thymus, which coincides with the onset and tissue site of V(D)J recombination of the TCR genes (15). Therefore, based on the expression pattern and DNA-binding specificity, we hypothesized that ZAS3 might play a role in lymphoid development. In support of this hypothesis, we showed that T-cell populations were developmentally impaired in *ZAS3*$^{-/-}$/*RAG2*$^{-/-}$ chimeric mice (9). Whereas the various T-cell compartments of *ZAS3*$^{-/-}$/*RAG2*$^{-/-}$ chimera were comparable to those of control mice at younger ages (less than 5 weeks old), there was a significant reduction in the CD4+CD8+ double positive compartment (8–24% of wild-type levels) in older (>6 months old) mice (2). These observations suggest that ZAS3 is not required for V(D)J recombination, but might be involved in T-cell survival or differentiation, possibly by affecting the frequency of specific gene segments for V(D)J recombination.

In order to quantitatively evaluate V(D)J recombination frequency, we compared the diversity of TCR-β chain in thymocytes between *ZAS3*$^{-/-}$ and control mice using a gene chip approach (32). The TCR-β

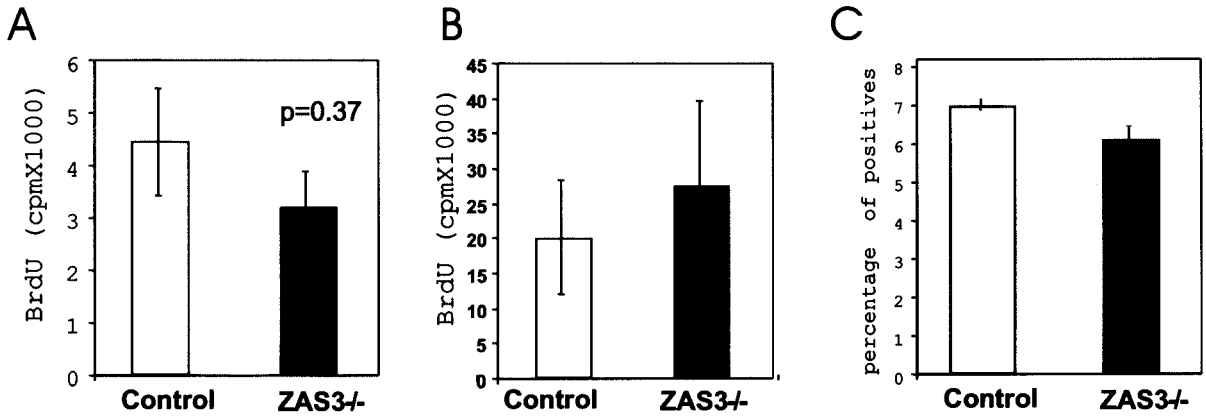

Figure 4. No significant differences in basal proliferation of endogenous thymocytes and splenocytes, and the diversity of the TCR-β chains between *ZAS3*$^{-/-}$ and wild-type mice. (A) CD4+ cells and (B) CD8+ BrdU incorporation. Control and *ZAS3*$^{-/-}$ mice were intraperitoneally injected with BrdU (1 mg), killed 3 h afterwards, and single-cell suspensions were prepared from thymus and spleen. The amount of BrdU incorporation was determined by flow cytometry according to the manufacturer's instructions (BD Pharmingen, San Diego, CA). (C) Analysis of TCR-β chain diversity using the gene chip method. TCR-β chain diversity was measured as described previously (32). Total RNA was isolated from two independent pairs of 2-month-old ZAS3 wild-type and knockout male siblings. The integrity of the RNA preparations was shown by absorbance ratios at 260–280 nm of ~2.0, and further verified with an Agilent Bioanalyzer. First-strand cDNAs were synthesized using a primer designed to bind the constant region of the TCR-β chain. Equal amounts of the in vitro transcription products (cRNAs) from each sample were hybridized to human genome U133A 2.0 gene chips (Affymetrix Inc., Santa Clara, CA), and then the data were analyzed as described in Materials and Methods. The quality control for background noise used for Affymetrix GeneChip image, which showed no background noise in these experiments, was shown by Raw Q values of ≥ 5.

chain was chosen here to reflect the T-cell repertoire because it confers the majority of TCR diversity (5). TCR-β-specific cRNAs generated by a primer complementary to the constant region of the TCR-β chain were hybridized to human genome U133A 2.0 Array. Human gene chips containing known but unselected expressed sequence tags from human genes were used because they should share less homology with mouse lymphocyte receptor RNA. The human sequences present on the array served as random sequence targets for the TCR-β probe. The number of positive signals above background from each thymocyte sample was counted and the percentages of positives, which reflected the level of diversity, was 6.9 ± 0.28 ($n = 2$) for the wild-type and 6.1 ± 0.84 ($n = 2$) for the mutant (Fig. 4C). Thus, there was no significant difference in the overall TCR-β diversity between the two groups. Although the lack of ZAS3 did not quantitatively affect the overall diversity of the TCR-β chain, we have not ruled out possible differences in the usage of individual antigen receptors in these mice.

Microarray Analysis of Whole Thymus Gene Expression

ZAS proteins have been shown to regulate transcription of specific target genes (45). A microarray strategy was used to evaluate the effects of deletion of ZAS3 on global expression in the thymus. Because we have demonstrated a rapid decline in ZAS3 expression in primary lymphocytes upon cultivation (Fig. 1), we cautiously extracted RNA from freshly isolated whole thymus from five pairs of wild-type and *ZAS3*$^{-/-}$ siblings. Corresponding pairs of sample cRNAs, synthesized and labeled with Cy3 (wild-type) or Cy5 (*ZAS3*$^{-/-}$) by reverse transcription, were hybridized to mouse oligo microarray (Agilent G4121A). Normalized data were analyzed with Gene Traffic™ software, and statistically significant changes in the expression of many genes were observed. Complete data tables are published on the GEO website (http://www.ncbi.nlm.nih.gov/entrez, accession number GSE6570). Genes whose expression was either up (206 genes; 1.0%) or down (262 genes; 1.2%) by a minimum of 1.5-fold and in at least four of the five array slides are shown in Supplemental Table 1A and 1B, respectively (supplemental tables available from Ohio State University departmental website: http://medicine.osu.edu/mcbiochem/Faculty%20Pages/Wu.html). Overall, the lack of ZAS3 led to subtle changes in the expression of relatively few genes. Only 25 genes (0.09%) were identified with increased expression more than twofold and 6 genes (0.03%) with decreased expression more than twofold. Reproducibility of the data from the individual array slides was verified using the NIA Array Analysis Tool with correlation coefficients for all experiments greater than 97%, indicating both high reproducibility and minimal influence of genetic variability (Table 2). Subsequently, the differential expression of a selected group of six ZAS3 candidate genes (Ephrin A1, NK2, glomulin, JAK1, Trim30, and RAG1) between ZAS3-null and wild-type thymi seen in microarray analysis was validated by real-time PCR experiments. The mRNA levels of all six genes tested showed a significant correlation between microarray and PCR data (Fig. 5). As a control, no significant difference in expression of GAPDH was observed between ZAS3-null and wild-type thymi.

To discern if any particular gene classes was significantly affected by the lack of ZAS3, the microarray data were submitted for analysis using the Expression Analysis Systematic Explorer (EASE) program (18), which identifies overrepresentation of gene categories that have similar functions within the array data sets. An EASE score is calculated for likelihood of overrepresentation of biological processes, molecular functions, and cellular component categories using the Gene Ontology (GO) database. Categories with an EASE score of <0.05 were determined to be significantly overrepresented. The predominant classes associated with ZAS3 deficiency in the thymus are shown in Table 3. Complete EASE results are listed in Supplementary Tables 2A and 2B (available at http://medicine.osu.edu/mcbiochem/Faculty%20Pages/Wu.html). The main class of genes that is upregulated (>1.5-fold) in ZAS3-null thymus belongs to the G-protein-coupled receptor proteins, including many individual olfactory receptor genes, and associated signaling molecules. Classes of genes that are downregulated in *ZAS3*$^{-/-}$ thymus are mostly involved in RNA, DNA, and nucleotide metabolism or binding. The functional implication of the EASE data remains to be established because the main classes of genes overrepresented in *ZAS3*$^{-/-}$ thymus have not

TABLE 2
CORRELATION MATRIX FOR ZAS3-NULL THYMUS MICROARRAY RESULTS

	1	2	3	4	5
1	1	0.972	0.987	0.982	0.991
2	0.972	1	0.977	0.981	0.98
3	0.987	0.977	1	0.99	0.989
4	0.982	0.981	0.99	1	0.991
5	0.991	0.98	0.989	0.991	1

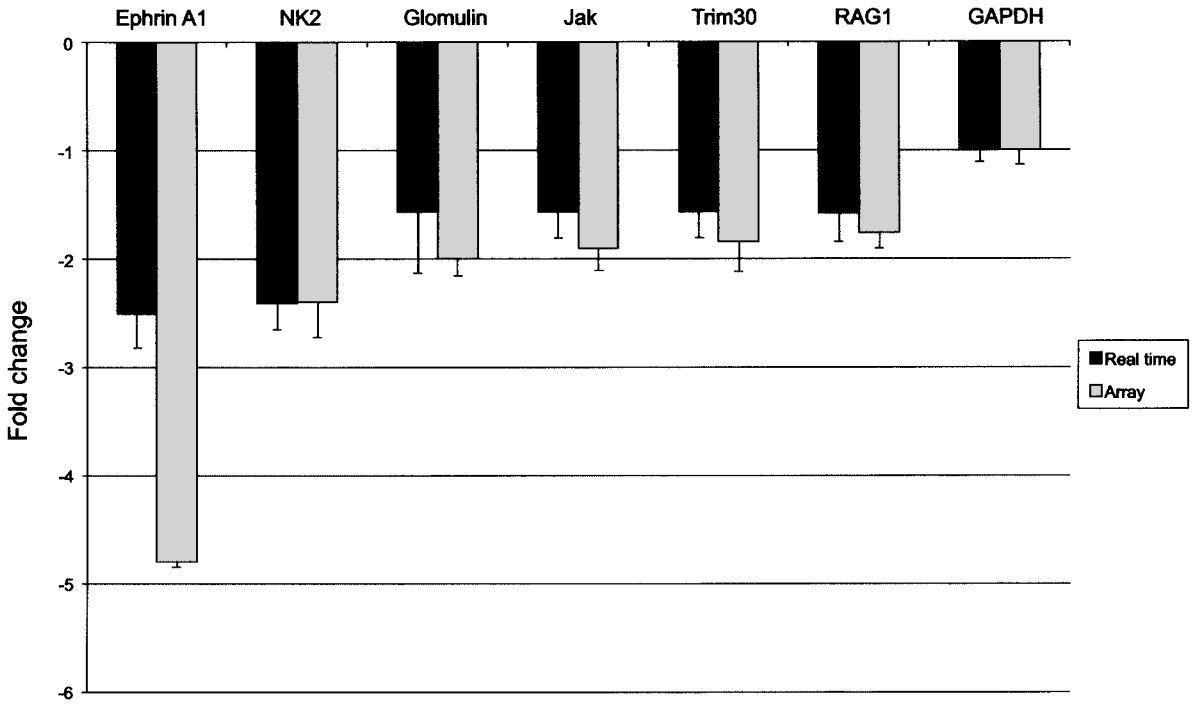

Figure 5. Quantitative real-time PCR analysis showed differential expression of selected transcripts between *ZAS3*$^{-/-}$ and wild-type thymocytes. Expression array results (shown in gray bars) were the average of five independent experiments. Data of real-time PCR (shown in black bars) were the average of three independent amplification experiments. The real-time PCR results were similar to those of the microarray data, which showed differential expression of these transcripts between *ZAS3*$^{-/-}$ and wild-type thymocytes.

TABLE 3
FUNCTIONAL GROUPS OF ZAS3-NULL THYMUS MICROARRAY RESULTS

	Gene Expression Increased >1.5-Fold (206 Genes)	Gene Expression Decreased >1.5-Fold (262 Genes)
GO categories significantly overrepresented		
G-protein-coupled receptor protein signaling pathway	24 genes (EASE score = 5.73E-04; FDR = 0)	
G-protein-coupled receptor activity	21 genes (EASE score = 2.15E-03; FDR = 0)	
Signal transducer activity	40 genes (EASE score = 3.79E-03; FDR = 0)	
Cell surface receptor linked with signal transduction	26 genes (EASE score = 7.03E-03; FDR = 0)	
Transmembrane receptor activity	24 genes (EASE score = 8.81E-03; FDR = 0)	
Rhodopsin-like receptor activity	17 genes (EASE score = 1.47E-02; FDR = 0)	
Cellular process	71 genes (EASE score = 1.90E-02; FDR = 0)	
Receptor activity	30 genes (EASE score = 2.09E-02; FDR = 0)	
GO categories significantly overrepresented		
RNA metabolism		12 genes (EASE score = 2.05E-03; FDR = 0)
Purine nucleotide binding		29 genes (EASE score = 3.22E-03; FDR = 0)
Adenyl nucleotide binding		25 genes (EASE score = 3.57E-03; FDR = 0)
Nucleotide binding		29 genes (EASE score = 3.96E-03; FDR = 0)
RNA processing		11 genes (EASE score = 4.11E-03; FDR = 0)
ATP binding		24 genes (EASE score = 6.21E-03; FDR = 0)
Cell cycle		15 genes (EASE score = 1.19E-02; FDR = 0)
Nucleic acid binding		43 genes (EASE score = 1.46E-02; FDR = 0)

been previously associated with ZAS3 or any ZAS proteins.

Altered Binding Affinity to NF-κB and AP-1 Sites in ZAS3-Null Tissues

Previous results show that ZAS3 regulates the function of NF-κB and AP-1 through protein–protein interactions in vitro. ZAS3 associates with TRAF2 to inhibit the nuclear translocation of the p65 subunit of NF-κB (17,34), and with c-Jun to regulate AP-1 activity and IL-2 expression (34). In EMSA performed with nuclear extracts of thymus, spleen, brain, and liver, and ^{32}P-labeled double strand oligonucleotides harboring a NF-κB binding site, three major κB–DNA–protein complexes were observed (Fig. 6A, upper panels), which correspond to p65/p50 heterodimers, p50 homodimers, and ZAS proteins in ascending order of gel mobility (17). Increased nuclear p65/p50 was observed in the spleen, brain, and liver of *ZAS3*$^{-/-}$ mice compared with control mice, whereas no significant changes in p50/p50 were observed (Fig. 6A, upper panel). Increased nuclear NF-κB in *ZAS3*$^{-/-}$ cells is consistent with a previous observation that showed constitutive activation of NF-κB in ZAS3-deficient pre-B cells and that ZAS3 inhibits the nuclear translocation of NF-κB (17). Additionally, a significant reduction in the fastest migrating complex was observed in *ZAS3*$^{-/-}$ thymus when compared to wild-type, suggesting the presence of ZAS3 in that complex. Evidence supporting the fastest migrating complex to contain ZAS3 includes antibody gel supershift assays and its absence in ZAS3-deficient B cells (17). This complex may persist in ZAS3-null cells due to probe bound by ubiquitously expressed ZAS1 and ZAS2 that also bind to NF-κB target sites (10,31).

Western blot analysis confirmed the EMSA data

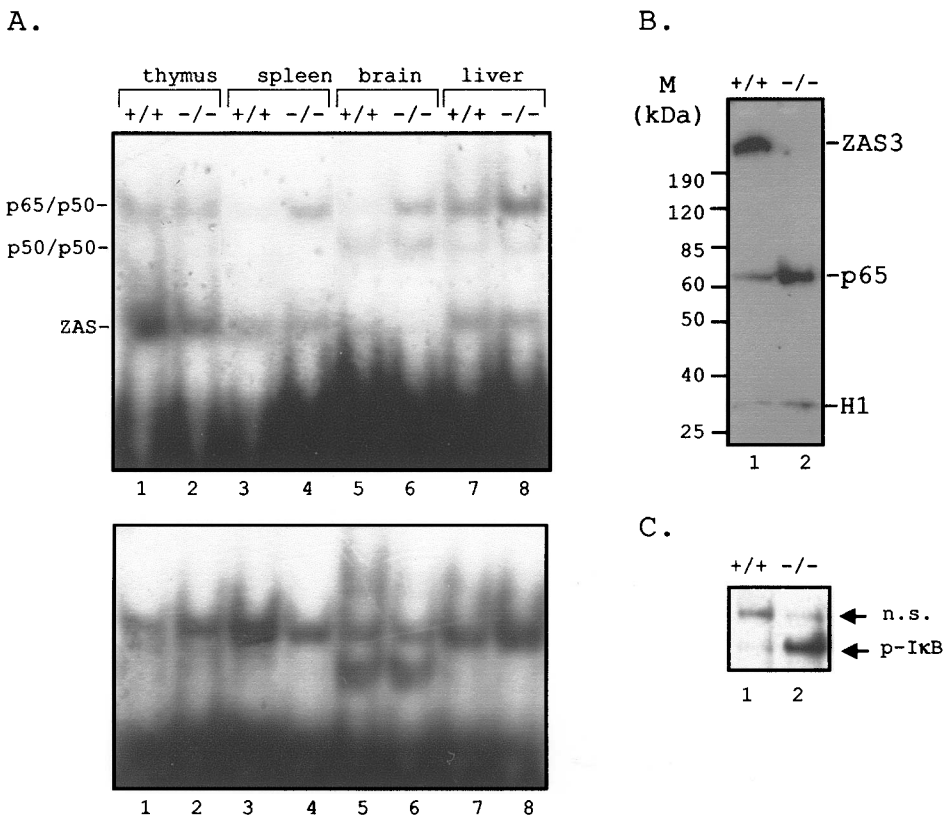

Figure 6. Alteration of NF-κB and AP-1 activity in *ZAS3*$^{-/-}$ mice. (A) EMSA of nuclear extracts prepared from various tissues of *ZAS3*$^{-/-}$ mice, wild-type *ZAS3*$^{+/+}$ control, and [^{32}P]κB oligonucleotides (upper panels), and [^{32}P]AP-1 oligonucleotides (lower panel). (B) Immunoblot analysis of nuclear extracts prepared from spleens of *ZAS3*$^{-/-}$ mice and wild-type *ZAS3*$^{+/+}$ control. Nuclear extracts (30 μg) were resolved by 4–20% SDS-PAGE and transferred onto PVDF membranes. Proteins membranes were incubated with ZAS3, p65, and histone H1 antibodies, washed, and then incubated with secondary antibodies conjugated with horseradish peroxidase. Signals were obtained by exposing protein filters to X-ray films. (C) Immunoblot analysis of protein extracts from spleen. Protein membranes prepared as in (B) using total protein extracts (30 μg) prepared from spleens of *ZAS3*$^{-/-}$ and control *ZAS3*$^{+/+}$ mice were hybridized with p-IκB antibodies. Equivalent protein loading was shown by staining the protein gels (E-Zinc Reversible Stain Kit, Pierce, Rockford, IL) before transferring proteins onto PVDF membranes. A nonspecific signal (n.s.) is shown to highlight the more intense signal yielded from p-IκB antibodies from the *ZAS3*$^{-/-}$ spleen sample.

showing increased nuclear p65/p50 binding activity in most tissues examined, with a three- to fourfold increase in nuclear p65 in spleens of *ZAS3*$^{-/-}$ mice compared to wild-type spleens (Fig. 6B). The 265-kDa ZAS3 protein was observed in the control but not in the *ZAS3*$^{-/-}$ sample, whereas histone H1 was present in both samples, showing equal protein loading (Fig. 6B). The decrease in p65 in the control samples relative to ZAS3-deficient samples may be at least in part due to the association of ZAS3 with TRAF2 to prevent the assembly of the IKK complex (17,33). IKK phosphorylates the NF-κB inhibitor IκB, which in turns leads to IκB ubquitination and degradation, and nuclear translocation of NF-κB. Western blot analysis showed increased phosphorylated IκB in *ZAS3*$^{-/-}$ spleen protein lysates compared to control (Fig. 6C). Therefore, the constitutive expression of NF-κB in *ZAS3*$^{-/-}$ mice provides direct physiological evidence that ZAS3 inhibits the nuclear translocation of NF-κB.

Concurrent EMSA using the same *ZAS3*$^{-/-}$ and wild-type samples showed tissue-specific differences in AP-1 binding activity (Fig. 6A, lower panels). Compared to wild-type controls, AP-1 binding activity was increased in thymus and liver, but decreased in spleen in nuclear extract of *ZAS3*$^{-/-}$ mice. A previous report showed that ZAS3 associates with c-Jun to activate AP-1 (34). Our data further suggest that ZAS3 may activate or inhibit AP-1 in a tissue-specific manner. Although the changes in the DNA binding of NF-κB and AP-1 in *ZAS3*$^{-/-}$ tissues was not always reciprocal, emerging evidence suggests that NF-κB inhibits AP-1, and vice versa. AP-1 recruits histone deacetylase, HDAC1, to repress NF-κB (24), whereas NF-κB upregulates the DNA damage protein GADD45β, a known inhibitor of JNK, and hence AP-1 (11). Our results suggest ZAS3 may participate in a dynamic interplay between NF-κB and AP-1 to modulate specific gene transcription, growth, and programmed cell death. Further analysis of ZAS3 knockout mice will allow more precise elucidation of tissue-specific role of ZAS3 in NF-κB- and AP-1-mediated transcription. Despite changes in DNA-binding affinity and cellular localization of these important transcriptional regulators, we observed relatively minor differences in global gene expression, as discussed above. This discrepancy may be due to redundant functions of other transcription factors.

Increased Peripheral Activated and Memory T Cells in ZAS3-Deficient Mice

T-cell development in spleen and thymus of 3-month-old *ZAS3*$^{-/-}$ mice was examined by flow cytometry. In the spleen, the relative numbers of splenocytes and T cells and the CD4+ and CD8+ subpopulations were comparable between wild-type and *ZAS3*$^{-/-}$ mice (Fig. 7A). However, there were significant differences in the expression levels of some functional markers in the CD4+ subset, but not in the CD8+ subset. Compared to control CD4+ splenocytes, in *ZAS3*$^{-/-}$ cells there was increased CD44^{hi}/CD62L^{lo} cells with a corresponding decreased CD44^{lo}/CD62L^{hi} subset (Fig. 7B). There was also increased CD25 (Fig. 7C) and CD69 expression in *ZAS3*$^{-/-}$ splenic CD4+ cells (Fig. 7D). Increased memory markers (CD44^{hi}/CD62L^{lo}) and increased activation markers (CD25 and CD69) in splenic CD4+ cells suggest that the peripheral ZAS3-null CD4+ populations have increased memory T-cell phenotypes. On the other hand, in the *ZAS3*$^{-/-}$ CD3+ thymocytes there was a decreased CD4+/CD8+ ratio (Fig. 8A) as well as decreased expression of the CD69 activation marker (Fig. 8B). Decreased CD69+ expression in TCR-β^{hi} cells was also observed in *ZAS2/Shn2*$^{-/-}$ and *ZAS2/Shn2*$^{+/-}$ thymocytes compared to wild-type cells (25). Given that there was a decreased CD3+CD4+ population in the thymus of *ZAS3*$^{-/-}$ mice, conversion to memory phenotype may have occurred in response to lymphopenia followed by homeostatic proliferation in peripheral T-cell compartments, similar to that occurring during the early postnatal period (28). The decreased expression of CD69 in thymocytes of *ZAS3* and *ZAS2/Shn-2* mice suggest a conserved and nonredundant function in regulating CD69 expression of the ZAS proteins. The changes in expression of the cell surface markers in *ZAS2* and *ZAS3* mice suggest the ZAS proteins are likely to be important regulators of T-cell development and function.

ZAS3-Deficient Mice Had Decreased Fertility and Increased Bone Density

Other notable phenotypes observed in the ZAS3-null mice include decreased fertility and progressive increase in bone density. ZAS3 mouse colonies have been maintained by intercrossing ZAS3 heterozygous mice. The litter size of offspring was normal, averaging eight pups per litter. From 247 offspring examined, the *ZAS3* +/+:+/–:–/– ratio was 1.12:1.96:0.92, which approximates the expected Mendelian ratio. Complete loss of ZAS3, however, led to a marked reduction in fertility in both male and female mice. So far, mating of female or male *ZAS3*$^{-/-}$ mice with *ZAS3*$^{+/-}$ or *ZAS3*$^{-/-}$ partners has only yielded one litter for each combination over more than 20 attempts. Additionally, the number of offspring produced from those mating was significantly fewer than normal,

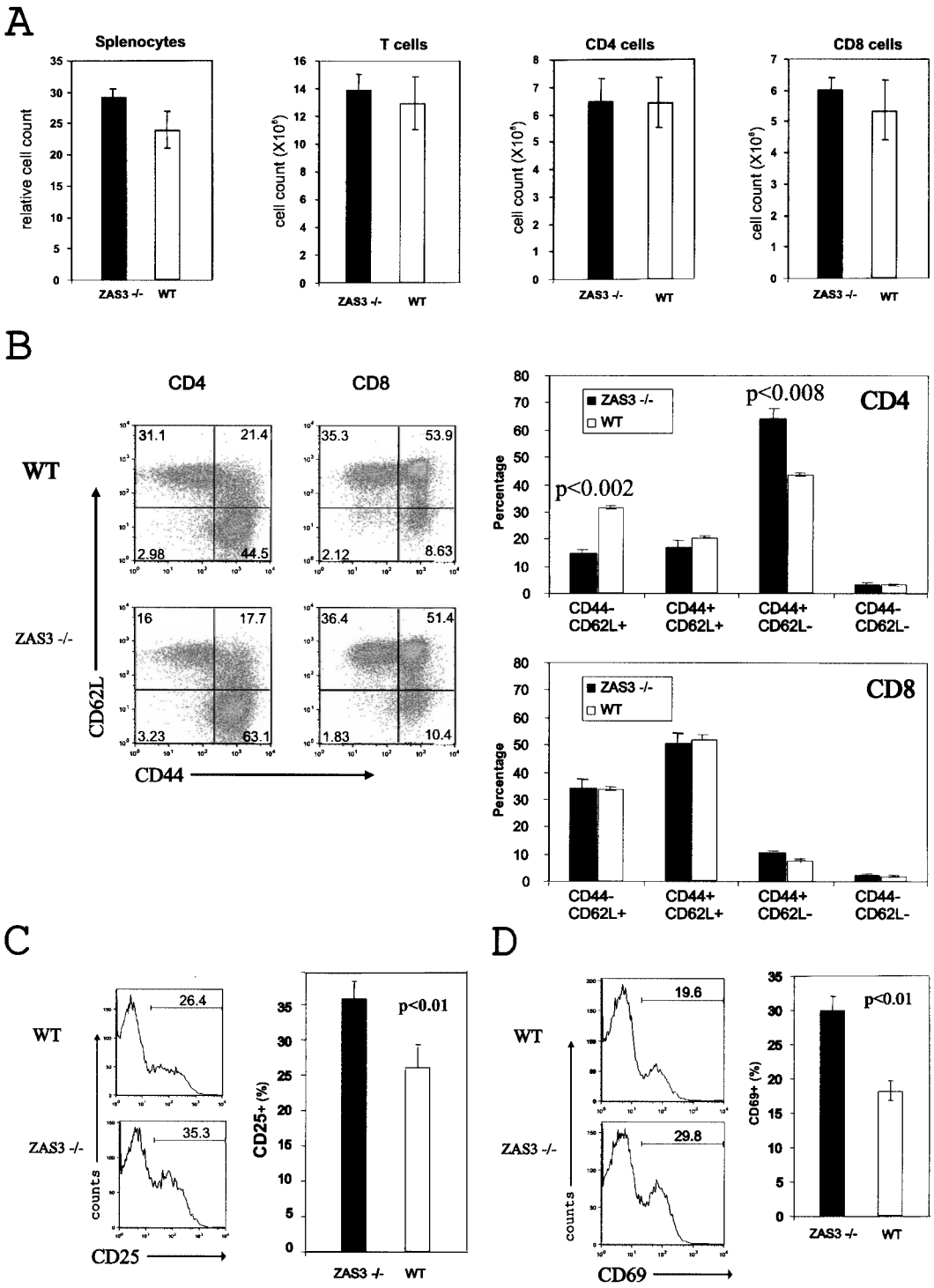

Figure 7. Increase in activated and memory phenotypes in splenic CD4 T cells of *ZAS3*$^{-/-}$ mice. (A) Bar charts comparing the number of splenocytes, total T cells, CD4+ and CD8+ cells between *ZAS3*$^{-/-}$ and *ZAS3*$^{+/+}$ control mice. (B) FACS analysis of surface expression of CD44 and CD62L in CD4+ or CD8+ T cells. Left panels representative two-parameter dot plots, and right panels are bar charts showing mean ± SEM ($n = 3$). (C) FACS analysis of CD25 surface expression in CD4+ splenocytes of *ZAS3*$^{-/-}$ and *ZAS3*$^{+/+}$ control mice. (D) FACS analysis of CD69 surface expression in CD4+ splenocytes of *ZAS3*$^{-/-}$ and *ZAS3*$^{+/+}$ control mice. Black bars: *ZAS3*$^{-/-}$; and white bars: wild-type control.

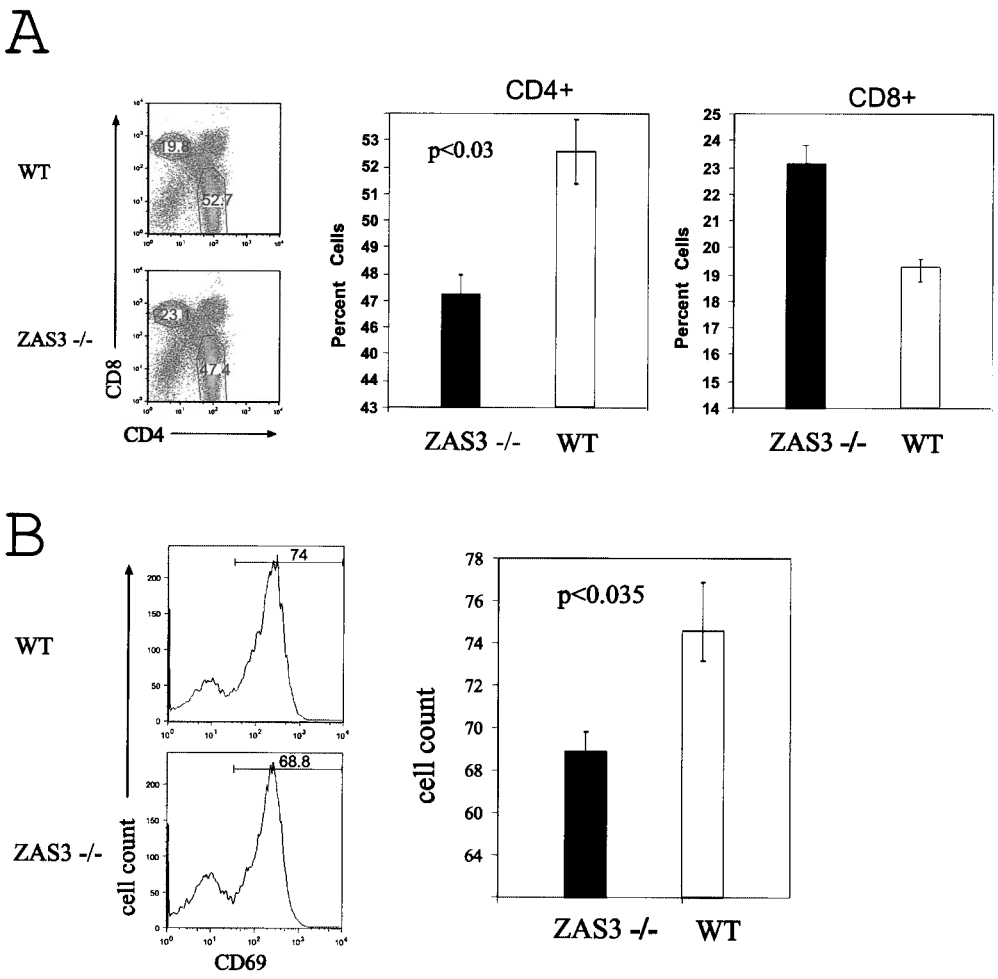

Figure 8. Decreased CD4 and CD69 expression in CD3+ thymocytes of *ZAS3*$^{-/-}$ mice. FACS analysis of cell surface expression of (A) CD4 and CD8; and (B) CD69 after gating on CD3+ cells ($n = 3$).

only four to six pups per litter, suggesting that ZAS3 may be important in fertility and embryonic development. There are precedents showing that the ZAS proteins are involved in reproduction. Schnurri restricts germ cell proliferation. Its deficiency caused formation of abnormal cysts, which contain excess number of cells that cannot differentiate into gametes. Furthermore, flies with null mutation of *shn* were sterile (27). For *ZAS2*$^{-/-}$ mice, female mice did not nurse their pups, and male mice had abnormal sexual behavior (42). Similarly, ZAS3 might be involved in the specific cell cycle alterations that occur during gametogenesis in mammals, probably through its growth inhibitory function partially via inhibition of NF-κB. However, the precise mechanism of reduced fertility in *ZAS3*$^{-/-}$ mice remains to be established.

In addition to decreased fertility, another finding in the *ZAS3*$^{-/-}$ mice was progressive increase in bone density as evidenced by radiographic studies of 7-month-old animals (Fig. 9A, B) and histological analyses of longitudinal bone sections (Fig. 9C). The amount of cancellous bone was clearly increased in the femur of ZAS3-deficient mice relative to that in the controls (Fig. 9C). The height of hypertrophic zone in the growth plate and the length of tibia and femur in both mice were comparable, indicating that ZAS3 deficiency had no effect on longitudinal bone growth.

Changes in bone mass and defects in bone remodeling have recently been reported in other ZAS genetic models, including ZAS2 (36) and ZAS3 (23). In contrast to increased bone density observed in *ZAS3*$^{-/-}$ mice, the *ZAS2*$^{-/-}$ mice had decreased bone density. ZAS2 activates bone remodeling by affecting both osteoblastic bone formation and osteoclastic bone resorption activities (36). Further studies show that ZAS2 modulates the activities of NFATc1 and c-fos, two crucial transcription factors required for normal bone remodeling (36). Jones et al. generated

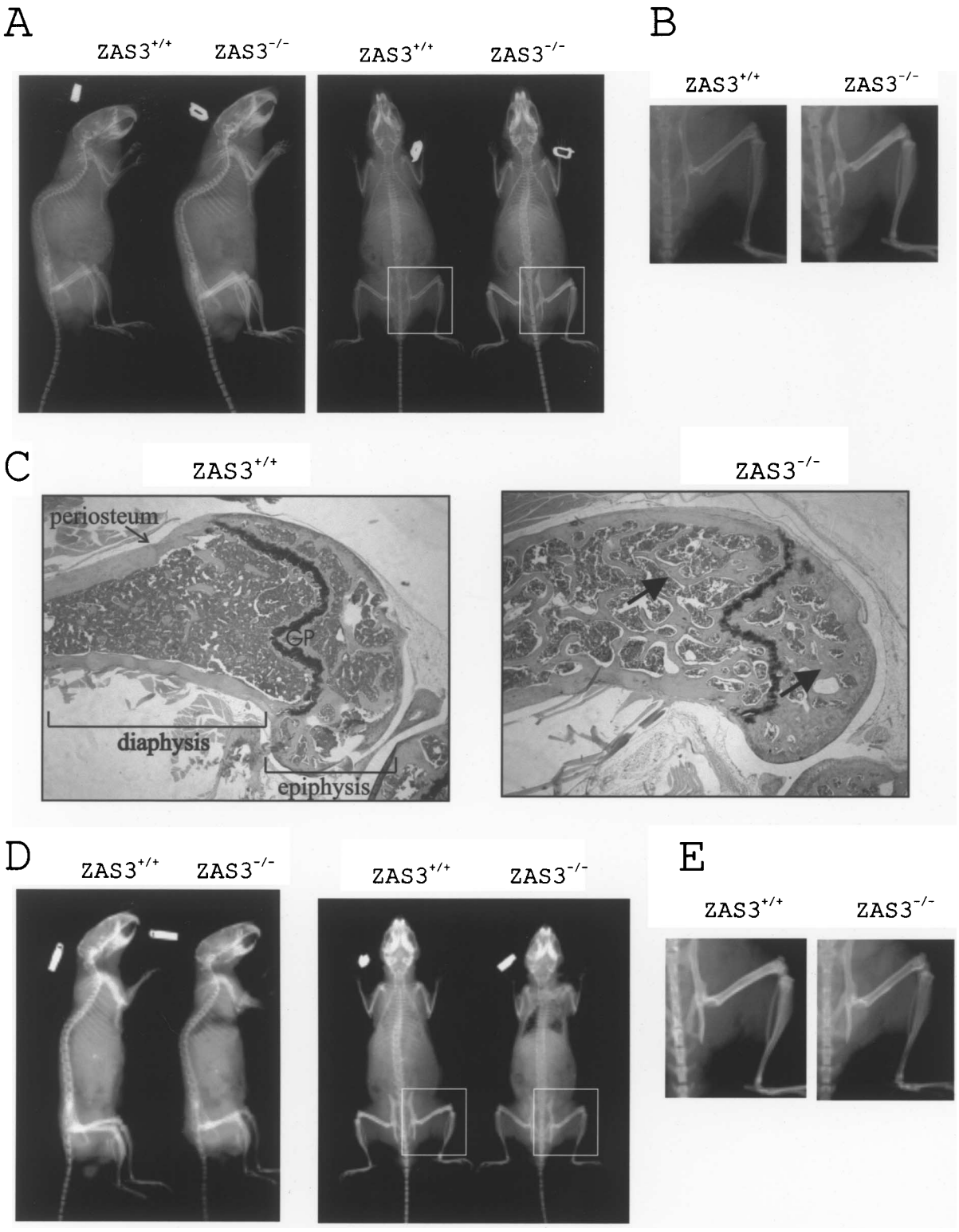

Figure 9. General increased bone density in *ZAS3*$^{-/-}$ mice. (A) Whole body radiological analysis. Seven-month old *ZAS3*$^{-/-}$ mice showed increased radiodensity of skull, jaw, long bones, and vertebrae compared to wild-type littermates. Lateral view shows successful eruption of incisor teeth (left panels) and anterior–posterior view (right panels). (B) Enlargement of the boxed areas in (A) to show the abnormal signal in the marrow space of the distal femur of a *ZAS3*$^{-/-}$ mouse. (C) Hematoxylin-stained sections of distal femur from 5-month-old littermate control (left) and *ZAS3*$^{-/-}$ mice (right). Only few trabecular bone elements were observed in the wild-type bone, whereas the density of trabecular bone (indicated with arrows) is greatly increased throughout diaphysis and epiphysis of *ZAS3*$^{-/-}$ femur. (D) Radiographs showing slight decreased in bone density in 3-month-old *ZAS3*$^{-/-}$ compared with *ZAS3*$^{+/+}$ littermate controls. (E) Enlargement of the boxed areas in (D) to show the femur of 3-month-old *ZAS3*$^{-/-}$ mouse was less dense than wild-type control.

Shn3/ZAS3-null mice by replacing a 5.5-kb region, containing exon 10, intron 10, and exon 11, with a neomycin resistance cassette (23). Although alteration in lymphoid development has not been reported in those *Shn3/ZAS3*-null mice, an osteosclerotic phenotype was observed (23). In those *Shn3/ZAS3*$^{-/-}$ mice, the thickening of skeletal architecture was observed as early as in 2-week-old mice (23). However, our *ZAS3*$^{-/-}$ mice did not exhibit such an early onset in bone thickening, and even showed a slight decrease in bone mass when they were 3 months old (Figs. 9D, E). Such discrepancy in bone thickness between the two *ZAS3*$^{-/-}$ mouse models is speculative, but may include differences in genetic background. Although *ZAS2*$^{-/-}$ mice had an overall reduction in bone mass as early as 1 week of age, 8-week-old mice showed increased cancellous bone limited to metaphyses (36). Unlike *ZAS2*$^{-/-}$ mice in which the defects in bone remodeling involves both osteoblasts and osteoclasts, the increased in bone mass in *Shn3/ZAS3*$^{-/-}$mice was attributed solely to enhanced osteoblast activity (23). Shn3/ZAS3 was found to control the protein levels of Runx2, the principal transcriptional regulator of osteoblast differentiation, by promoting its degradation through recruitment of the E3 ubiquitin ligase WWP1 to Runx2 (23). Thus, ZAS2 and ZAS3 appear to exert opposite effect on bone development and do so through different mechanisms: transcription regulation of NFATc1 andc-fos by ZAS2 (36), and posttranslational destabilization of Runx2 by Shn3/ZAS3 (23).

Notably, *Runx2* was identified in our whole thymus microarray analysis as one of the very few genes whose expression was significantly decreased (1.94-fold) in the ZAS3-null thymus. In the thymus, Runx2 can interfere with early T-cell development, cause an expansion of a specific subset, and predispose to lymphoma (8). We speculate that ZAS3 may affect Runx2 function in thymus as it does in osteoblasts. Decreased *Runx2* transcripts in *ZAS3*$^{-/-}$ mice suggest ZAS3 might also affect the transcription of *Runx2* and/or stability of Runx2 transcripts. In addition to Runx2, other known ZAS-associated proteins, such as TGF-β/BMP family of proteins, play roles in bone development [reviewed in (26)]. Interestingly, the Runx family of transcription factors physically interact in some TGF-β signaling pathways (21,29). Furthermore, ZAS-regulated transcription factors, NF-κB and AP-1, have important roles as key regulators of bone development. Double-knockout mice lacking both the p50 and p52 subunits of NF-κB developed osteopetrosis with the absence of osteoclasts (20,49). Likewise, transgenic mice expressing dominant-negative c-Jun specifically in the osteoclast lineage manifested severe osteopetrosis due to impaired osteoclastogenesis (19). It is possible that the TGF-β, NF-κB, and AP-1 protein families together orchestrate the osteosclerotic phenotype in the ZAS3-null mice. Despite the progressive increase in bone density, there were no congenital bony abnormalities or obvious differences in limb function or mobility in our *ZAS3*$^{-/-}$ animals.

CONCLUSIONS

Due to rapid loss of ZAS3 expression in primary lymphocytes within 24 h during in vitro cultivation, we generated *ZAS3*$^{-/-}$ mice to study the physiological function of the ZAS proteins. Whereas disruption of *shn*, the single *Drosophila ZAS* homologue, is embryonic lethal, individual *ZAS* knockout mice are viable. Likely, the ZAS proteins have overlapping and/or compensatory functions. The identification of ZAS target genes using the animal models is essential to shed light on physiological function of the ZAS proteins. Although the defects of *ZAS2*$^{-/-}$ or *ZAS3*$^{-/-}$ mice are not severe, they involve diverse physiological processes, including lymphoid development, bone remodeling, behavior, and reproduction. Apparently, the ZAS proteins can regulate multiple cellular pathways through both transcriptional and posttranslational mechanisms. Besides direct regulation of gene transcription through specific DNA binding, the ZAS proteins are involved in cell signaling through protein–protein interaction in multiple pathways, including NF-κB, AP-1, TGF-β, and Runx2. Because the ZAS proteins are large, more than 2500 amino acids, and contains two acidic regions for protein–protein interactions and multiple zinc fingers, we propose that the ZAS proteins could serve as a scaffold where important cellular machineries are assembled. Targeted disruption of two or more ZAS genes to overcome redundant gene function will be essential to study the ZAS protein family in future.

REFERENCES

1. Allen, C. E.; Mak, C. H.; Wu, L. C. The kappa B transcriptional enhancer motif and signal sequences of V(D)J recombination are targets for the zinc finger protein HIVEP3/KRC: A site selection amplification binding study. BMC Immunol. 3:10; 2002.
2. Allen, C. E.; Muthusamy, N.; Weisbrode, S. E.; Hong, J. W.; Wu, L. C. Developmental anomalies and neoplasia in animals and cells deficient in the large zinc finger protein KRC. Genes Chromosomes Cancer 35: 287–298; 2002.

3. Allen, C. E.; Wu, L. C. Downregulation of KRC induces proliferation; anchorage independence; and mitotic cell death in HeLa cells. Exp. Cell Res. 260:346–356; 2000.
4. Allen, C. E.; Wu, L. C. ZAS zinc finger proteins: The other κB-binding protein family. In: Iuchi S.; Kuldell, N., eds. Zinc finger proteins: From atomic contact to cellular function. Georgetown, TX: Landes Bioscience; 2005:207–214.
5. Arstila, T. P.; Casrouge, A.; Baron, V.; Even, J.; Kanellopoulos, J.; Kourilsky, P. A direct estimate of the human alphabeta T cell receptor diversity. Science 286:958–961; 1999.
6. Bachmeyer, C.; Mak, C. H.; Yu, C. Y.; Wu, L. C. Regulation by phosphorylation of the zinc finger protein KRC that binds the kappaB motif and V(D)J recombination signal sequences. Nucleic Acids Res. 27:643–648; 1999.
7. Baldwin, Sr., A. S. The NF-kappa B and I kappa B proteins: New discoveries and insights. Annu. Rev. Immunol. 14:649–683; 1996.
8. Blyth, K.; Vaillant, F.; Hanlon, L.; Mackay, N.; Bell, M.; Jenkins, A. J.; Neil, C.; Cameron, E. R. Runx2 and MYC collaborate in lymphoma development by suppressing apoptotic and growth arrest pathways in vivo. Cancer Res. 66:2195–2201; 2006.
9. Chen, J.; Lansford, R.; Stewart, V.; Young, F.; Alt, F. W. RAG-2-deficient blastocyst complementation: An assay of gene function in lymphocyte development. Proc. Natl. Acad. Sci. USA 90:4528–4532; 1993.
10. Dorflinger, U.; Pscherer, A.; Moser, M.; Rummele, P.; Schule, R.; Buettner, R. Activation of somatostatin receptor II expression by transcription factors MIBP1 and SEF-2 in the murine brain. Mol. Cell Biol. 19: 3736–3747; 1999.
11. Eliseev, R. A.; Zuscik, M. J.; Schwarz, E. M.; O'Keefe, R. J.; Drissi, H.; Rosier, R. N. Increased radiation-induced apoptosis of Saos2 cells via inhibition of NFkappaB: A role for c-Jun N-terminal kinase. J. Cell Biochem. 96:1262–1273; 2005.
12. Falt, S.; Holmberg, K.; Lambert, B.; Wennborg, A. Long-term global gene expression patterns in irradiated human lymphocytes. Carcinogenesis 24:1837–1845; 2003.
13. Foehr, M. L.; Lindy, A. S.; Fairbank, R. C.; Amin, N. M.; Xu, M.; Yanowitz, J.; Fire, A. Z.; Liu, J. An antagonistic role for the *C. elegans* Schnurri homolog SMA-9 in modulating TGF{beta} signaling during mesodermal patterning. Development 133:2887–2896; 2006.
14. Fugmann, S. D.; Lee, A. I.; Shockett, P. E.; Villey, I. J.; Schatz, D. G. The RAG proteins and V(D)J recombination: Complexes; ends; and transposition. Annu. Rev. Immunol. 18:495–527; 2000.
15. Hicar, M. D.; Robinson, M. L.; Wu, L. C. Embryonic expression and regulation of the large zinc finger protein KRC. Genesis 33:8–20; 2002.
16. Hogan, B. Manipulating the mouse embryo: A laboratory manual, 2nd ed. Plainview, NY: Cold Spring Harbor Laboratory Press; 1994.
17. Hong, J. W.; Allen, C. E.; Wu, L. C. Inhibition of NF-kappaB by ZAS3; a zinc-finger protein that also binds to the kappaB motif. Proc. Natl. Acad. Sci. USA 100: 12301–12306; 2003.
18. Hosack, D. A.; Dennis, Jr., G.; Sherman, B. T.; Lane, H. C.; Lempicki, R. A. Identifying biological themes within lists of genes with EASE. Genome Biol. 4:R70; 2003.
19. Ikeda, F.; Nishimura, R.; Matsubara, T.; et al. Critical roles of c-Jun signaling in regulation of NFAT family and RANKL-regulated osteoclast differentiation. J. Clin. Invest. 114:475–484; 2004.
20. Iotsova, V.; Caamano, J.; Loy, J.; Yang, Y.; Lewin, A.; Bravo, R. Osteopetrosis in mice lacking NF-kappaB1 and NF-kappaB2. Nat. Med. 3:1285–1289; 1997.
21. Ito, Y.; Miyazono, K. RUNX transcription factors as key targets of TGF-beta superfamily signaling. Curr. Opin. Genet. Dev. 13:43–47; 2003.
22. Jin, W.; Takagi, T.; Kanesashi, S. N.; et al. Schnurri-2 controls BMP-dependent adipogenesis via interaction with Smad proteins. Dev. Cell 10:461–471; 2006.
23. Jones, D. C.; Wein, M. N.; Oukka, M.; Hofstaetter, J. G.; Glimcher, M. J.; Glimcher, L. H. Regulation of adult bone mass by the zinc finger adapter protein Schnurri-3. Science 312:1223–1227; 2006.
24. Kim, T.; Yoon, J.; Cho, H.; et al. Downregulation of lipopolysaccharide response in *Drosophila* by negative crosstalk between the AP1 and NF-kappaB signaling modules. Nat. Immunol. 6:211–218; 2005.
25. Kimura, M. Y.; Hosokawa, H.; Yamashita, M.; et al. Regulation of T helper type 2 cell differentiation by murine Schnurri-2. J. Exp. Med. 201:397–408; 2005.
26. Li, X.; Cao, X. BMP signaling and skeletogenesis. Ann. NY Acad. Sci. 1068:26–40; 2006.
27. Matunis, E.; Tran, J.; Gonczy, P.; Caldwell, K.; DiNardo, S. punt and schnurri regulate a somatically derived signal that restricts proliferation of committed progenitors in the germline. Development 124:4383–4391; 1997.
28. Min, B.; McHugh, R.; Sempowski, G. D.; Mackall, C.; Foucras, G.; Paul, W. E. Neonates support lymphopenia-induced proliferation. Immunity 18:131–140; 2003.
29. Miyazaki, H.; Watabe, T.; Kitamura, T.; Miyazono, K. BMP signals inhibit proliferation and in vivo tumor growth of androgen-insensitive prostate carcinoma cells. Oncogene 23:9326–9335; 2004.
30. Montagutelli, X. Effect of the genetic background on the phenotype of mouse mutations. J. Am. Soc. Nephrol. 11(Suppl. 16):S101–105; 2000.
31. Nakamura, T.; Donovan, D. M.; Hamada, K.; et al. Regulation of the mouse alpha A-crystallin gene: Isolation of a cDNA encoding a protein that binds to a cis sequence motif shared with the major histocompatibility complex class I gene and other genes. Mol. Cell. Biol. 10:3700–3708; 1990.
32. Ogle, B. M.; Cascalho, M.; Joao, C.; Taylor, W.; West, L. J.; Platt, J. L. Direct measurement of lymphocyte receptor diversity. Nucleic Acids Res. 31:e139; 2003.
33. Oukka, M.; Kim, S. T.; Lugo, G.; Sun, J.; Wu, L. C.;

Glimcher, L. H. A mammalian homolog of *Drosophila* schnurri, KRC, regulates TNF receptor-driven responses and interacts with TRAF2. Mol. Cell 9:121–131; 2002.
34. Oukka, M.; Wein, M. N.; Glimcher, L. H. Schnurri-3 (KRC) interacts with c-Jun to regulate the IL-2 gene in T cells. J. Exp. Med. 199:15–24; 2004.
35. Richards, J. O.; Chang, X.; Blaser, B. W.; Caligiuri, M. A.; Zheng, P.; Liu, Y. Tumor growth impedes natural-killer-cell maturation in the bone marrow. Blood 108:246–252; 2006.
36. Saita, Y.; Takagi, T.; Kitahara, K.; et al. Lack of schnurri-2 expression associates with reduced bone remodeling and osteopenia. J. Biol. Chem. 17:12907–12915; 2007.
37. Savage-Dunn, C.; Maduzia, L. L.; Zimmerman, C. M.; et al. Genetic screen for small body size mutants in *C. elegans* reveals many TGFbeta pathway components. Genesis 35:239–247; 2003.
38. Shivdasani, A. A.; Ingham, P. W. Regulation of stem cell maintenance and transit amplifying cell proliferation by tgf-beta signaling in Drosophila spermatogenesis. Curr. Biol. 13:2065–2072; 2003.
39. Sung, T. L.; Rice, A. P. Effects of prostratin on cyclin T1/P-TEFb function and the gene expression profile in primary resting CD4+ T cells. Retrovirology 3:66; 2006.
40. Suzuki, T.; Minehata, K.; Akagi, K.; Jenkins, N. A.; Copeland, N. G. Tumor suppressor gene identification using retroviral insertional mutagenesis in Blm-deficient mice. EMBO J. 25:3422–3431; 2006.
41. Takagi, T.; Harada, J.; Ishii, S. Murine Schnurri-2 is required for positive selection of thymocytes. Nat. Immunol. 2:1048–1053; 2001.
42. Takagi, T.; Jin, W.; Taya, K.; Watanabe, G.; Mori, K.; Ishii, S. Schnurri-2 mutant mice are hypersensitive to stress and hyperactive. Brain Res. 1108:88–97; 2006.
43. Torres-Vazquez, J.; Park, S.; Warrior, R.; Arora, K. The transcription factor Schnurri plays a dual role in mediating Dpp signaling during embryogenesis. Development 128:1657–1670; 2001.
44. Torres-Vazquez, J.; Warrior, R.; Arora, K. schnurri is required for dpp-dependent patterning of the *Drosophila* wing. Dev. Biol. 227:388–402; 2000.
45. Wu, L. C. ZAS: C2H2 zinc finger proteins involved in growth and development. Gene Expr. 10:137–152; 2002.
46. Wu, L. C.; Hicar, M. D.; Hong, J.; Allen, C. E. The DNA-binding ability of HIVEP3/KRC decreases upon activation of V(D)J recombination. Immunogenetics 53:564–571; 2001.
47. Wu, L. C.; Mak, C. H.; Dear, N.; Boehm, T.; Foroni, L.; Rabbitts, T. H. Molecular cloning of a zinc finger protein which binds to the heptamer of the signal sequence for V(D)J recombination. Nucleic Acids Res. 21:5067–5073; 1993.
48. Yao, L. C.; Blitz, I. L.; Peiffer, D. A.; et al. Schnurri transcription factors from *Drosophila* and vertebrates can mediate Bmp signaling through a phylogenetically conserved mechanism. Development 133:4025–4034; 2006.
49. Zhang, Y. H.; Heulsmann, A.; Tondravi, M. M.; Mukherjee, A.; Abu-Amer, Y. Tumor necrosis factor-alpha (TNF) stimulates RANKL-induced osteoclastogenesis via coupling of TNF type 1 receptor and RANK signaling pathways. J. Biol. Chem. 276:563–568; 2001.